IMPEDANCE BASED FLOW RECONSTRUCTION — A NOVEL FLOW COMPOSITION MEASURING TECHNIQUE FOR MULTI-PHASE FLOWS

F. Klug; F. Mayinger
Lehrstuhl A f. Thermodynamik, Techn. Univ. München, FRG
Arcisstr. 21, 8000 München 2
Tel. 089/2105 3246, Fax. 2105 3451

ABSTRACT The new measuring technique (I F R) presented in this paper consists of a completely non-intrusive impedance probe and has been designed originally for offshore oil production. Nevertheless, it can be applied to the wide field of multi-phase flows, covering component ratios in the range of 0...100% over multiple flow regimes. It allows the on-line determination of the local volumetric concentrations of the flow components within the sensing volume with an accuracy better 2% and indicates the occuring flow regime. The reconstruction principle is described, and measured data for oil, water and gas flows are presented.

1.Introduction

The impedance method is a widely applied method for measurement of volumetric concentrations in multi-component flows. It is based on the different electrical properties (permittivity, conductivity) of the flow components and their effect on the measured impedance (capacitance, conductance) of an appropriate sensor. The majority of these applications comes from the field of two-phase flows, and especially from capacitance measurement in non-conducting fluids. Although the impedance method offers a number of advantages like simultaneous response and no need for moving parts, its sensitivity to the flow pattern sometimes restricts its application. Many different electrode designs have been developed, trying to minimize this limitation. A popular method is the use of parallel plate electrodes Auracher et.al.[1], the use of ring electrodes is described by Özgü et.al.[2]. Helical electrodes are described by Geraets et.al.[3], Abouelwafa et.al.[4]. A method of electrode excitation was proposed by Merilo et.al.[5] and incorporates the use of 6 strip- electrodes fed by a 3-phase voltage generator.

For the generally occuring flow conditions, especially with dispersed flow components, a number of analytical formulae are known, which connect the permittivity ε^* of a mixture of two fluids of particular permittivities ε_1, ε_2 with their volumetric concentration ratio. These models are based on general conditions regarding the shape of the dispersed particles and often are limited to relatively small maximum concentrations. The most popular models are those by e.g. Maxwell [6], Bruggemann [7], a very good review is given by van Beek [8]. Dykesteen et.al.[9] have proposed a method of determining the component concentrations in 3-component flows by measuring both the capacitance and the resistance of an impedance sensor.

The sensitivity of the impedance to the distribution pattern of the components within the sensor leads to different calibration curves for each flow regime. In many practical flow situations, these curves differ very much. In order to avoid large errors, this calls for more information about the dominating flow pattern.

2.New Approach

To overcome the insufficiencies mentioned above, a new approach is made for concentration measurement in multi-phase flows. Although the proposed method has been originally developed with respect to offshore applications in oil/water/gas-mixtures, it can be easily applied to a much wider field of multi-component flows. The main part of the described measurement setup is a non-intrusive impedance probe consisting of eight surface-plate electrodes mounted on the inner side of the tube (see fig.1). Each of the electrodes can be connected as a guard and/or measuring electrode respectively, so that a variety of shapes of the electrical field can be generated, which can be rotated around the probe center. Fig. 2 shows the undisturbed equipoten-

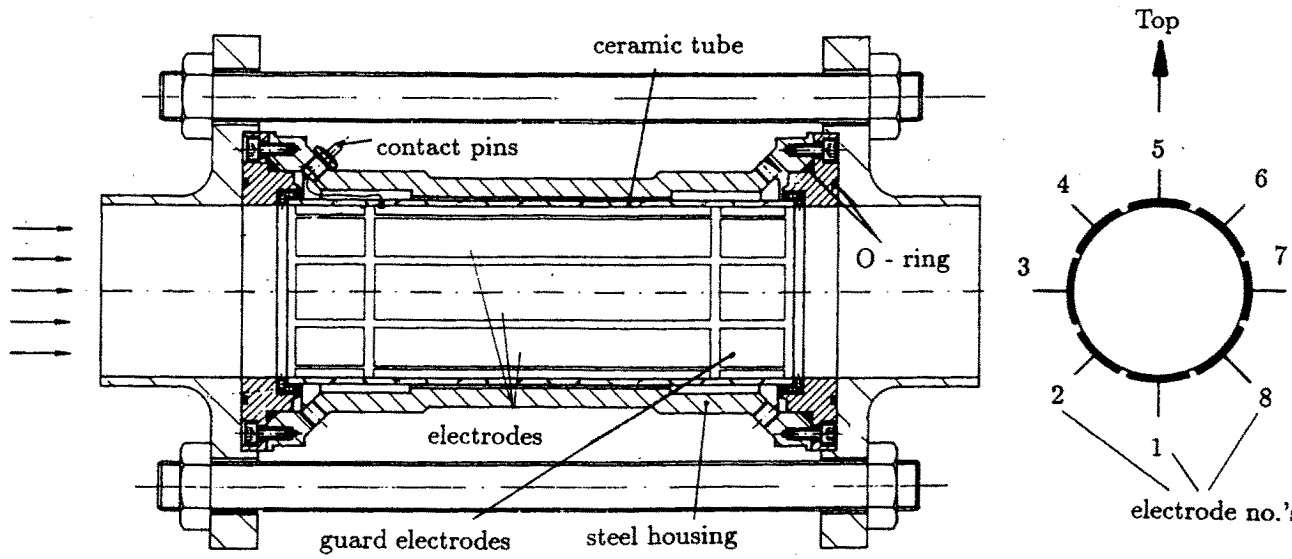

Fig. 1 : *Non- intrusive impedance probe (Ø54 mm, L= 160 mm) with 8 surface-plate electrodes.*

tial plots for the most important electrode potential configurations and the symbols for the derived measurement fields. Although the impedance is an integral parameter which is influenced by the component distribution within the whole sensing volume of the probe, there are characteristic sensitivity distribution patterns — indicated by the density of the equipotential lines — which allow to classify the variety of fields into several groups. These are the diametral fields $D_1 \dots D_4$, eccentric $E_1 \dots E_8$, wall $W_1 \dots W_8$ and large fields $B_1 \dots B_4$, integral fields I_1, I_2, and the Maltese-cross shaped field M_1. The different number of fields in each class arises from their different degree of symmetry. The almost homogeneous diametral fields $D_1 \dots D_4$ offer an impedance reading, that represents the component distribution along a narrow beam across the probe. The large fields $B_1 \dots B_4$ are similar, with a larger beam width, however. Going towards the eccentric $E_1 \dots E_8$ and wall fields $W_1 \dots W_8$, the field becomes more inhomogeneous and the sensitive area is moved from the center towards the outer regions. Fields I_1 and I_2 offer an average reading along the pipe circumference, which is still more emphasized by field M_1.

With the help of these fields, specific informations about the component distribution within the probe are collected, which allow for the reconstruction of the flow regime and the calculation of the component concentrations.

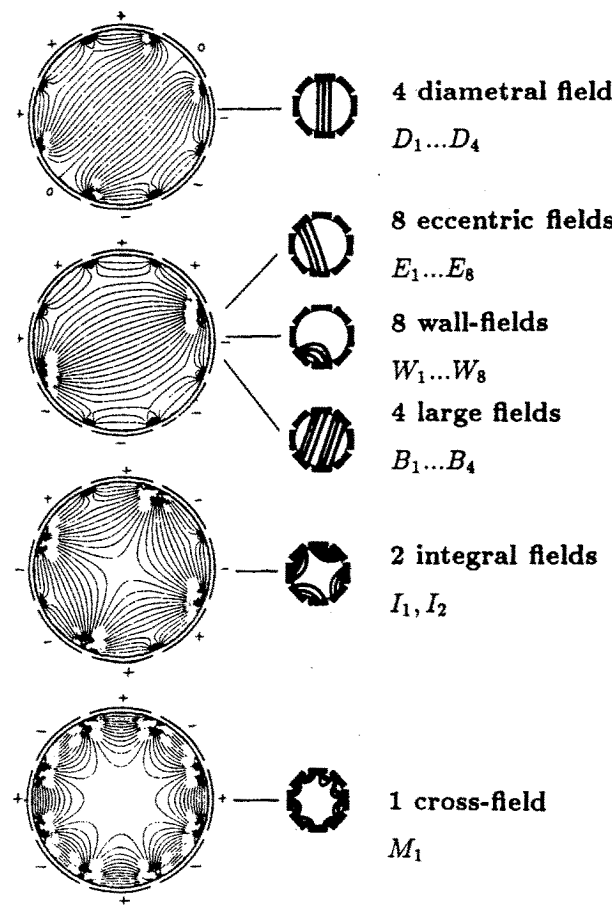

Fig. 2 : *Basic electrode potential distributions with derived measuring field shapes.*

3.Numerical impedance computation

In the general case of distributed flow components within the probe, an analytical expression for the probe impedance cannot be given. Therefore, the impedances between arbitrarily given electrodes as a function of the flow pattern and the applied field have to be calculated numerically. The electrostatic potential distribution within a region A of permittivity ϵ bounded by a rim S is described by Poisson's equation

$$\nabla^2\varphi = \Delta\varphi = -\frac{\varrho}{\varepsilon} \tag{1}$$

which in the special case, with no free charges ϱ, reduces to Laplace's equation

$$\Delta\varphi = 0 \tag{2}$$

where Δ stands for the Laplace operator and φ describes the potential. In cartesian coordinates, and if one of the three dimensions can be regarded infinite, eqn. (2) simplifies to the expression

$$\frac{\partial^2\varphi}{\partial x^2} + \frac{\partial^2\varphi}{\partial y^2} = 0 \tag{3}$$

In the general case, with distributed non- conducting flow components, the region A consists of subregions A_i with particular permittivities ε_i, and eqn. (3) holds within each subregion A_i. The conditions for material boundaries can be derived from the conservation laws for the tangential electric field intensity E_t and the normal flux density D_n

$$E_{t1} = E_{t2} \tag{4}$$

$$D_{n1} = D_{n2} \tag{5}$$

By applying the relation

$$\varepsilon \cdot E = D \tag{6}$$

the additional conditions

$$\frac{E_{n1}}{E_{n2}} = \frac{\varepsilon_2}{\varepsilon_1} \tag{7}$$

$$\frac{D_{t1}}{D_{t2}} = \frac{\varepsilon_1}{\varepsilon_2} \tag{8}$$

are obtained. The calculation of the two- dimensional field is accomplished by use of the finite-difference-method FDM [10]. A rectangular grid is generated over the total area A, and the conditions for material boundaries (eqns. (7,8)) and the general field law (eqn. (3)) have to be implemented. The boundary conditions (b.c.) along the rim S are as follows: electrodes are tied to fixed potential and must thus be treated as Dirichlet b.c.'s, while Neumann b.c.'s must be applied upon the spacings between the electrodes.

Provided, that the mesh width of the applied grid is fine enough and numerical errors are controlled, the above given set of equations is sufficient to calculate the potential distribution in an arbitrarily shaped impedance probe for any given component distribution. Fig. 3 shows numerically computed equipotential plots for simulated stratified and annular flows. It can be clearly seen, how the presence of water influences and bends the potential lines and thus changes the particular impedances between the electrodes.

The capacitance C_{AB} between any two of a given set of electrodes is determined by the existing electrical field between the assembly, i.e., by the potential distribution between the electrodes. From the computed potential distribution, the potential gradient normal to the electrodes can be taken for the calculation of the charge densities on the electrodes. The total charge Q_{AB} induced by electrode B on electrode A is given by integration of the charge density over the surface area of electrode A. According to the definition of capacitance,

$$C_{AB} = \frac{Q_{AB}}{\varphi_B - \varphi_A} \tag{9}$$

the capacitance between the two regarded electrodes is then obtained by division of the induced charge Q_{AB} by the potential difference.

In the case of non-conducting fluids, the impedance is only represented by a capacitance term, which can be calculated by the procedure given above. However, if at least one of the flow components is electrically conducting, a general expression for the impedance is essential, comprising the capacitance C and the conductance G. This step is done by using the complex permittivity

$$\lambda = \sigma + j\omega\varepsilon \tag{10}$$

instead of the real permittivity ε. In eqn. (10), σ denotes the specific conductivity while ω represents the angular frequency of the applied electrical a.c. field. The numerical field computation in this case has to be performed for both the real and the imaginary parts. In this way, the impedances between any electrodes can be calculated for every specified flow distribution within the probe, so that the distribution of the impedances for every measuring field is obtained.

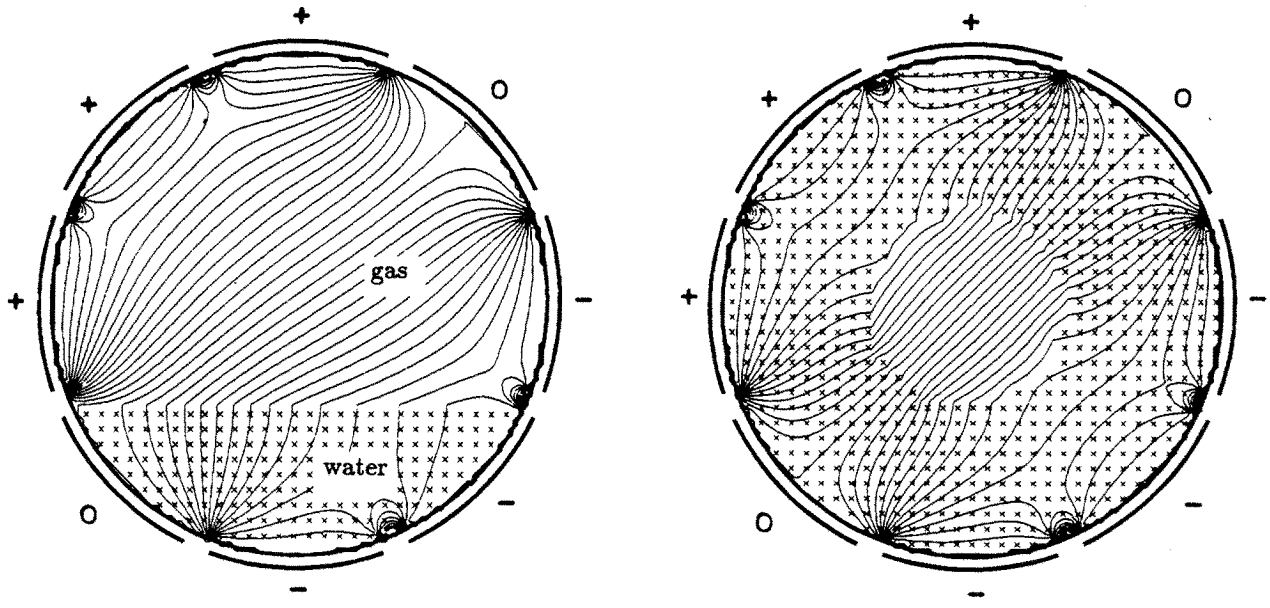

Fig. 3 : *Influence of the flow regime on the electric field, shown for stratified (left) and annular flow (right) of water and gas.*

4.Reconstruction Procedure

The reconstruction procedure is first explained for 2-component flows, e.g. oil/ gas. Here, the data of each measuring cycle consist of m capacitance readings C, corresponding to the m applied field shapes. These data are regarded as an m-dimensional vector V and compared to a stored reference Matrix M of dimension m x n. M consists of the m·n capacitance values numerically calculated before for n different flow compositions, covering several flow regimes. Within every flow regime, the component concentration is increased gradually, the stepwidth depending on the overall accuracy of the measurement setup (typ. 2%). In this way, the column numbers contain the encoded information about the flow composition and the flow regime.

The reconstruction of the flow regime and the component concentrations is accomplished by comparing V with the columns of M and determining the best- fit column. This can be achieved by several procedures, which calculate the error s(j) for each column and determine its minimum. A suitable procedure is the sum over error squares

$$s^*(j) = \sum_{i=1}^{m} (V_i - M_{ij})^2 \qquad (10)$$

However, in order to ensure a good comparability and to achieve independence of the actual probe dimensions, M and V are composed of relative capacitances C^*

$$C^* = \frac{C - C_{min}}{C_{max} - C_{min}} \qquad (11)$$

This leads to small errors in the range $s(j) < 1$ over most interesting flow regimes. In this region, the sum over absolute error roots,

$$s(j) = \sum_{i=1}^{m} (\mid V_i - M_{ij} \mid)^{\frac{1}{2}} \qquad (12)$$

shows a sharper detection of the minimum than equn. (10). The flow regime and the component concentration are then determined by decoding the address of the such determined best-fit column j_0.

In the case of oil/ water/ gas- flows, the two parameters void fraction α and water fraction β have to be determined simultaneously. This can be done by measuring both capacitance and conductance of the flow and also extending the reference matrix M towards the conductance data. In this case, the size of M is furthermore increased by the number of possible and reasonable combinations of α and β. With the accuracy given above, corresponding to 50 concentration steps for each component, an upper limit of 50 x 50 x 1/2 = 1250 columns for each flow regime is set for M.

5.Measurement Setup

The measurement setup with the essential components is shown in Fig. 4. It consists of the non-intrusive impedance probe, whose 8 surface plate electrodes are connected via a multiplexer switch MUX to a precision Impedance Meter LCR (Hewlett Packard 4284A). This instrument allows a fast measurement of the probe capitance and conductance over the frequency range from 20 Hz to 1 MHz at a typical accuracy of 0.05% . The voltages for the guard electrodes are generated by a pair of wideband driver amplifiers with a very low output impedance, driven by the impedance meter. The timing of the measurement cycles is controlled by the scanning control block implemented in a personal computer PC, which also acts as a data acquisition system with IEEE-Bus interface. Thus, the PC controls the switching of the desired field shape, then triggers the impedance measurement and reads the measured data. Data evaluation, i.e. the reconstruction of the flow composition and calculation of volumetric concentrations, is performed by the PC, too.

With this setup, the required time for one measurement cycle comprising the described 27 fields is less than 0.85 s, including the transmission of the data to the PC. The scanning time is nearly proportional to the number of applied fields. Therefore, the measurement rate of the setup can be considerably speeded up, if the flow regime is known and the number of required measuring fields can be significantly reduced.

At present, the total measurement speed is currently limited mainly by the LCR- meter ($\approx$ 30 ms per reading), while the calculation time for the reconstruction can be neglected in 2-phase flows.

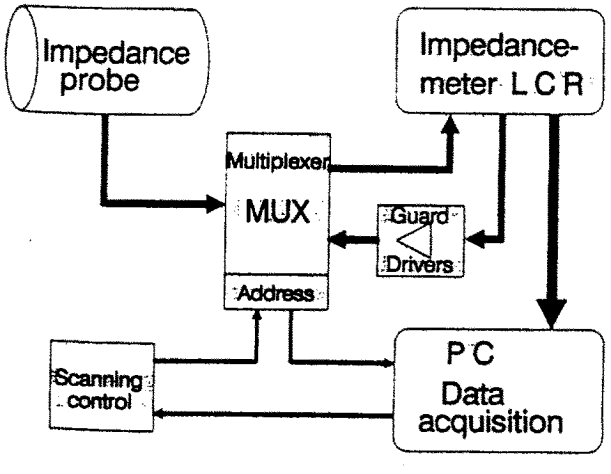

Fig. 4 : *Block diagram of the measurement setup.*

6.Experimental data

The experimental data shown below have been obtained with an impedance probe —Ø54 mm, l=160 mm — in steady flow conditions. To provide a purely capacitance measurement, the electrodes have been covered with a thin insulating layer of epoxy resin. This allows for the measurement in oil and water without the need for compensation for electrode polarisation impedances. The measurements were carried out in oil/ gas and water/ gas flows with tap water and SHELL / ONDINA 15 oil, void fraction ranging from $1 \geq \alpha \geq 0$

The measured capacitance data cover more than one order of magnitude, between diametral fields in oil/ gas ($8 \leq C \leq 10$ pF) and cross field in water/ gas ($50 \leq C \leq 330$ pF) and have therefore been converted into relative capacitance data (equn. 11).

In the 3-d-plots of fig. 5, the measured, relative capacitance distribution of the reference matrix is shown for the annular flow (AF), core flow (CF) and stratified flow (SF) regimes. The data (oil / gas) were measured for the indicated 27 field shapes and a total of 10 void fraction steps in each flow regime. The capacitance distributions for the axisymmetric AF and CF regimes show almost similar behaviour within each group of fields, the small discrepancies are caused by the manufacturing tolerances of the impedance probe. However, in the SF regime, this symmetry is broken and the fields within each group carry a more individual load of information.

The good performance of the reconstruction procedure is shown in fig. 6. The curves indicate the course of the error calculation according to the roots formula eqn.(12) for 3 measured capacitance vectors out of the AF, CF and SF regimes, respectively. The calculation of the error s(j) for each vector was based on a reference matrix containing a total of 75 columns over the AF, CF and SF regimes. Within each regime, the void fraction decreases in 25 steps from 1 to 0. The detected minima for each vector are unambiguous and show a safe distance to possible minima within other flow regimes. With this reconstruction procedure, the void fraction is determined with an accuracy of better than 2%.

Fig. 7 shows the capacitance distribution for the wall fields $W_1 \ldots W_8$, extracted from the reference matrix (fig.5) for SF regime. If the difference between lower and upper wall fields $\Delta C = C^*_{W1} - C^*_{W4}$ exceeds a significant limit (typ. 0.2), this can be used as a very safe indicator for the SF regime, see fig.8. With $\Delta C \geq 0.2$, the SF regime is indicated over a void fraction range of $0.05 \leq \alpha \leq 0.95$, while $\Delta C \approx 0$ occurs in all flow regimes with axisymmetric component distribu-

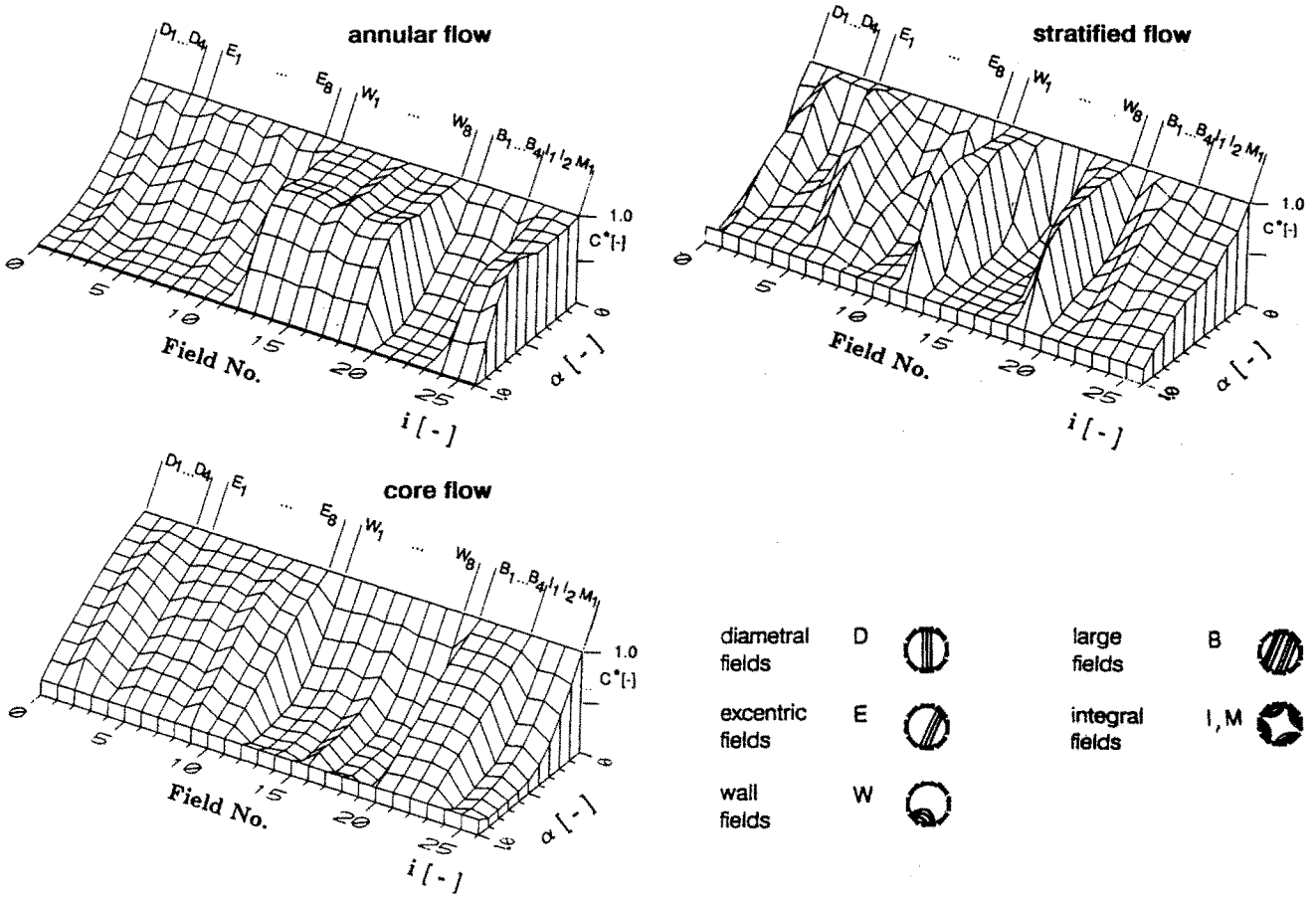

Fig. 5 : *Measured capacitance distribution of the reference matrix for the AF, CF, and SF regimes (oil/ gas) and void fraction steps of 10%*

tion. In contrast to the highly nonlinear behaviour of the wall fields, the integral fields I_1, I_2 and the cross field M_1 offer a much better suitability for void fraction calculation, caused by the averaging effect of these field shapes. Fig.9 shows the relative capacitance for these fields, measured in water/gas flows. These data (figs.7...9) show the possibility of setting up a considerably simplified measurement strategy for the SF regime. By using fields W_1 and W_4 as indicators and field I_1 for the calculation of α, the number of fields can be reduced from 27 down to 3, thus increasing the measurement rate by the factor 9 to over 10 frames/s. For the range of intermittent, sluggy flows in horizontal pipes, this offers a good resolution for the tracking of the void fraction.

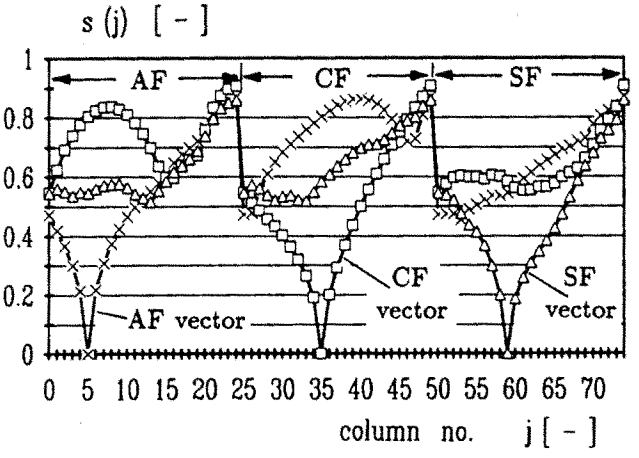

Fig. 6 : *Error s(j) (equn. 12) vs. column no. j of the reference matrix for measured data of AF, CF and SF regimes. Best-fit columns are detected at the minima of s(j).*

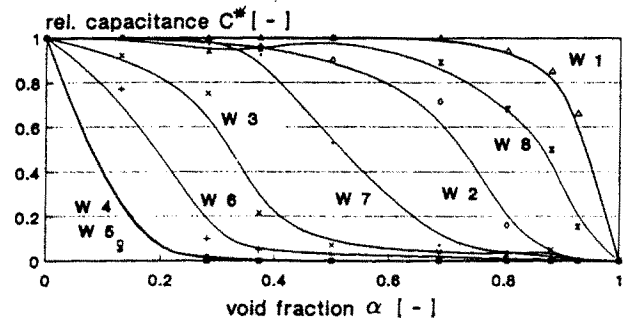

Fig. 7 : *Measured capacitance vs. void fraction for the wall-fields W1 ... W8 in SF regime of oil and gas.*

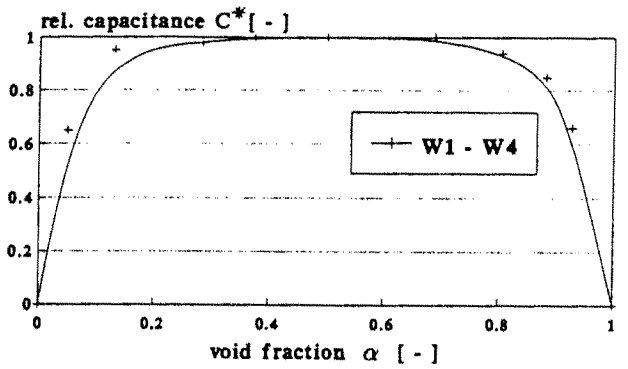

Fig. 8 : *Measured capacitance difference between wall-fields W4 and W1 vs. void fraction for SF regime of oil and gas.*

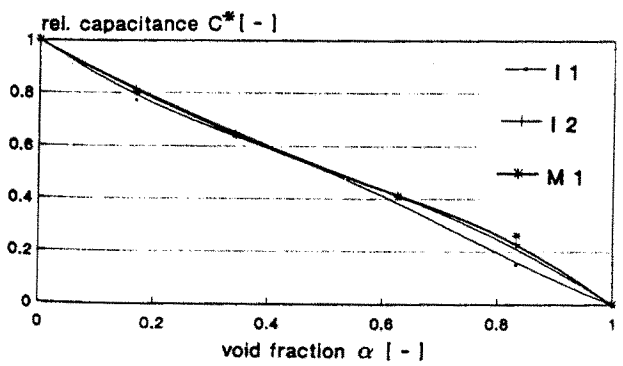

Fig. 9 : *Measured capacitance vs. void fraction for the integral (I1, I2) and cross- fields (M1) in SF regime of oil and water.*

7.Discussion and conclusions

Current works aim towards a further optimization of the measurement strategies as it was already pointed out for the SF regime. This includes the use of dedicated scanning cycles with a maximum load of characteristics for each flow regime, in order to minimize the number m of necessary measurements and the scanning time. Another point of interest is the optimization of the electrode length. With long electrodes, the measured data are more accurate and the spatial filtering effect leads to a better smoothing of the data. On the other hand, short electrodes offer a fast response and thus a good tracking of the temporal void fraction changes occuring in the slug flow regime.

Furthermore, work is concentrated on optimizing the reconstruction procedure for three-component flows. Although the measurement rate of the impedance meter is not decreased by the simultaneous measurement of capacitance and conductance, the calculation time required for the reconstruction is raised by the increased size of the reference matrix.

Combining the described method with a cross-correlation velocity measurement, a completely non- intrusive flow meter for a wide range of multi- component flows can be realized. For this reason, two identical, short impedance probes are located in a short distance along the pipe axis. The flow inhomogeneities generate two likely signals, shifted towards each other by a delay time τ, which can be calculated by cross- correlating both signals. Dividing the probe distance by τ yields the transport velocity of the flow.

References

[1] **Auracher, H.; Daubert, J.(1985):**
A capacitance method for void fraction measurements in two-phase flow. 2nd Int. Conf. on Multi-Phase Flow, London

[2] **Özgü, M.R.; Chen, J.C.(1973):**
A capacitance method for measurement of film thickness in two-phase flow. Rev. Sci. Instrum., Vol. 44, No. 12, pp. 1714-1716

[3] **Geraets, J.M.; Borst, J.C.(1988):**
A capacitance sensor for two-phase void fraction measurement and flow pattern identification. Int.J.-Multiphase flow, Vol.14, No.3, pp.305-320

[4] **Abouelwafa, M.; Kendall, J.M.(1980):**
The use of capacitance sensors for phase percentage determination in multiphase pipelines. IEEE Trans. Instr. Meas., Vol.IM-29, No.1, pp.24-27

[5] **Merilo, M. et.al.(1977):**
Void fraction measurement with a rotating electric field conductance gauge. Trans. ASME J.Heat Transfer Vol. 99, pp.330-332

[6] **Maxwell, J.C. (1892):**
A Treatise on Electricity and Magnetism, Vol.1, p. 452, Clarendon Press, Oxford

[7] **Bruggeman, D.A.G.(1935):**
Berechnung verschiedener physikalischer Konstanten von heterogenen Substanzen. Ann.d.Physik, Vol.24,No.5, pp.636-679

[8] **van Beek, L.K. (1967):**
Dielectric Behaviour of Heterogeneous Systems. Progress in Dielectrics, Vol 7.

[9] **Dykesteen, E. et al. (1985):**
Non-intrusive three-component ratio measurement using an impedance sensor. J. Phys. E.: Sci.-Instrum. Vol.18, pp.540-544.

[10] **Philippow, E. (1989):**
Grundlagen der Elektrotechnik. 8. Aufl., Hüthig Verlag, Heidelberg, 1989.

Used symbols

A		region
C	[F]	capacitance
C^*	[-]	rel. capacitance
D	$[As/m^2]$	flux density
E	[V/m]	field strength
G	$[\Omega^{-1}]$	conductance
M		matrix
Q	[As]	charge
S		rim of region A
V		vector
s		error value
l	[m]	length of probe
Ø	[m]	diameter of probe
x,y		cartesian coordinates
α	[-]	void fraction
β	[-]	water fraction
ε	[-]	permittivity
λ		complex permittivity
ϱ	$[Asm^{-3}]$	space-charge density
σ	$[\Omega^{-1}m^{-1}]$	specific conductivity
τ	[s]	delay (transit) time
φ	[V]	potential
ω	$[s^{-1}]$	angular frequency

Indices

i	row
j	column
A	electrode
B	electrode